

# Analytical and Experimental Analysis of a High Temperature Mercury Thermosyphon

**André Felipe Vieira da Cunha**

Assistant Researcher

**Marcia B. H. Mantelli**

Professor

Department of Mechanical Engineering,  
Heat Pipe Laboratory (LABTUCAL),  
Federal University of Santa Catarina,  
Florianópolis, SC 88040-970, Brazil

*High temperature thermosyphons are devices designed to operate at temperatures above 400°C. They can be applied in many industrial applications, including heat recovery from high temperature air fluxes. After a short literature review, which shows a deficiency of models for liquid metal thermosyphons, an analytical model, developed to predict the temperature distribution and the overall thermal resistance, is shown. In this model, the thermosyphon is divided into seven regions: three regions for the condensed liquid, including the condenser, adiabatic region, and evaporator; one region for vapor; one for the liquid pool; one for the noncondensable gases; and another for the tube wall. The condensation phenomenon is modeled according to the Nusselt theory for condensation in vertical walls. Numerical methods are used to solve the resulting equations and to determine the temperature distribution in the tube wall. Ideal gas law is applied for the noncondensable gases inside the thermosyphon, while the evaporator and condenser heat transfer coefficients are obtained from literature correlations. Experimental tests are conducted for thermosyphon with mercury as working fluid, designed and constructed in the laboratory. The results for two thermosyphons with different geometry configurations are tested: one made of a finned tube in the condenser region and another of a smooth tube. The finned tube presents lower wall temperature levels when compared with the smooth tube. The experimental data are compared with the proposed model for two different liquid pool heat transfer coefficients. It is observed that the comparison between the experimental data and theoretical temperature profiles is good for the condenser region. For the evaporator, where two distinct regions are observed (liquid film and pool), the comparison is not so good, independent of the heat transfer coefficient used. In a general sense, the model has proved to be a useful tool for the design of liquid metal thermosyphons. [DOI: 10.1115/1.3089551]*

**Keywords:** thermosyphon, high temperature, liquid metal, mercury, heat pipe

## 1 Introduction

Thermosyphons are high thermal conductance devices able to transfer high amount of heat. In its most simple form, a thermosyphon is an evacuated metal pipe, charged with a predetermined volume of an appropriate working fluid. It can be divided into three main sections: evaporator, where heat is delivered to the device, an adiabatic section (which can or cannot exist), and a condenser, where the transferred heat is released. In the evaporator section, heat evaporates the working fluid. Usually two subregions are found in the thermosyphon evaporator: a liquid film, attached to the tube wall and a pool on the bottom of the device. The vapor generated in the evaporator moves toward the condenser region, where it condenses, and the condensed liquid returns to the evaporator by gravity.

High temperature thermosyphons work at temperatures above 400°C. They can be applied for industrial equipment. One good example is regenerative heat exchangers in petroleum plants assisted by thermosyphons. This equipment is used to recover heat from high temperature streams, such as those released from furnaces, and uses the energy to preheat air.

The usual working fluids for high temperature thermosyphons are liquid metals, including potassium, sodium, mercury, or lithium. Table 1 shows the melting and boiling points of these materials and the range of operation temperatures of the thermo-

syphons [1]. They present good heat transfer characteristics: high thermal conductivities, high heats of vaporization, and high surface tension coefficients. However, sodium, potassium, and lithium are elements that require careful handling. They are highly reactive with water and humidity, liberating flammable gases. On the other hand, mercury is a highly toxic substance and has been avoided in thermosyphons for industrial applications.

The tube material must be chemically compatible with the working fluid to avoid chemical reactions, which could produce undesirable noncondensable gases. The material of the tubes must also resist corrosion, keeping its mechanical properties at the high working temperatures. In this work, stainless steel was used to manufacture the mercury thermosyphons that attend well the temperature range of this working fluid. Alternative materials for thermosyphons are ceramics, such as silicon carbide and alumina. These materials have excellent corrosion and erosion resistances and high strength in high temperature. Some working fluids, such as lithium, are not compatible with ceramic materials [2]. Therefore, ceramic pipes should be provided with a protective inner liner, which matches with the ceramic expansion characteristics.

Ranken and Lundberg [2] described some high temperature ceramic heat pipes. The authors discussed the deposition of a metal layer in the inner wall to prevent corrosion of the pipe by the liquid metal. The following combinations between tube material and protective layers were studied: alumina/niobium and silicon carbide/tungsten. Note that the alumina and silicon carbide have different chemical and physical properties. Sodium and lithium were used as the working fluid in both cases.

Merrigan [3] initially conducted experiments of alumina heat pipes with sodium as the working fluid. The alumina case was

Contributed by the Heat Transfer Division of ASME for publication in the JOURNAL OF HEAT TRANSFER. Manuscript received April 24, 2008; final manuscript received January 29, 2009; published online June 22, 2009. Review conducted by Yutaka Asako.

**Table 1 Melting and boiling points of liquid metals at atmospheric pressure (1 atm)**

Working fluids	Melting point (°C)	Boiling point (°C)	Usual range (°C)
Sodium	98	892	600–1200
Lithium	179	1340	1000–1800
Potassium	62	774	500–1000
Mercury	–39	357	300–600

used due to the low cost and safe operation without protective metal. None of the heat pipes tested survived the thermal shock imposed during the operation startup. The first successful operation of Merrigan [3] with high temperature heat pipes was observed for silicon carbide heat pipes using a protective layer of tungsten. The working fluid was sodium, operating in air and flue gas at temperatures of around 927°C. After 100 h of operation and 30 start-up cycles, the tube was sectioned and examined to verify the presence of some deterioration and corrosion. The corrosion of tungsten by sodium was considered acceptable.

The main objective of the present study is to develop technologies for high temperature thermosyphons aiming at industrial equipment applications, such as heat exchangers for chemical and petroleum industries. Therefore, a complete easy to handle analytical model to predict the temperature distribution and the heat transfer capacity of liquid metal thermosyphons is developed. Also, experimental studies are conducted to produce data that are compared with model results.

In this work, thermosyphons and heat pipes are considered as different devices. Thermosyphons use gravity to return the condensate to the evaporator, while heat pipes employ capillary forces provided by its internal porous media.

## 2 Literature Review

Yamamoto et al. [4] conducted one of the first studies in high temperature heat pipes with screen mesh porous media. They investigated the lifetime and performance of stainless steel case heat pipes with sodium as the working fluid. These heat pipes were subjected to temperatures levels of 600°C, 650°C, and 700°C for 1200 h of operation, with the condenser exposed to the environment. After each test, each heat pipe was cut, and its inner surface and screen mesh were analyzed. A small corrosion was observed. Other literature experimental works concerning high temperature thermosyphons and heat pipes include Refs. [5–7].

Yamamoto et al. [5] conducted an experimental study about mercury thermosyphons and heat pipes. The tested tubes were exposed to temperatures between 350°C and 600°C. The temperature profile along the tube was measured. The tubes reached the steady state conditions in about 30 h. After the completion of the tests, the materials of the internal sections were analyzed, and the authors concluded that the metal corrosion was small.

Reid et al. [6] manufactured heat pipes using lithium as the working fluid and molybdenum as the tube material. They tested the tube in horizontal orientation. The heat pipe was able to achieve 1400 K above the room temperature in 20 min.

Park and Boo [7] developed an experimental apparatus to analyze the performance of heat pipes using sodium as the working fluid. The evaporator region was heated by means of an electric furnace. The tube was manufactured with 316L stainless steel. They observed that the temperature distribution depended on the heat transfer rate of the device.

Few studies in the literature involve analytical or numerical models for predicting the performance of thermosyphons. This is particularly true for liquid metal thermosyphons. Reed [8] and Reed and Tien [9] presented an analytical model for the thermal performance of thermosyphons, but the working fluid was not liquid metal. Their model is based on mass, momentum, and en-

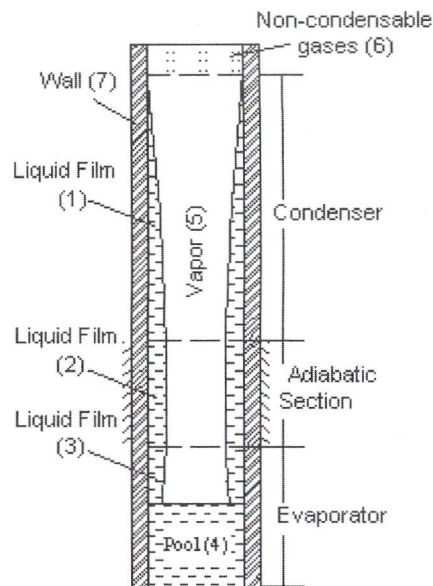


**Fig. 1 Schematic high temperature thermosyphon model**

ergy balances for the vapor and for the liquid film, in several sections of the thermosyphon. The objective of the model was to determine the operation characteristics of this device, including the liquid film thickness, the mass flow rate, and temperature of vapor, as well as to provide the drying and flooding limits. Both transient and steady regimes were analyzed.

Storey [10] modeled numerically the operation of a water thermosyphon in the transient regime. The numerical model includes conduction of the wall, the shear stress between the vapor and liquid film, the influence of the liquid mass in the pool, and the effective length due to the expansion and contraction of noncondensable gases in the vapor nucleus. The model assumes one-dimensional flow of the vapor and of the condensed liquid film, and two-dimensional conduction of wall. The transient behavior in the liquid pool was also modeled.

Ling and Cao [11] analyzed miniature high temperature rotating heat pipes by employing appropriate flow and heat transfer models. To obtain data to compare with the model, they performed an experimental investigation of these devices. The effects of noncondensable gases on temperature distribution along heat pipe length were also investigated. They concluded that these noncondensable gases have adverse effect on the heat pipe performance, resulting in a large temperature gradient near the condenser end, reducing the heat pipe heat transfer capacity. Their models consider zero heat transfer coefficients between the noncondensable gas region and case wall. Therefore, only conduction heat transfer is considered in this region.

Harley and Faghri [12] presented a transient two-dimensional thermosyphon model that accounts for conjugate heat transfer through the wall and the falling condensate film. The vapor flow and pipe wall regions were solved by complete transient two-dimensional conservation equations, and the liquid film was modeled using a quasisteady Nusselt-type solution. This model does not consider the effects of noncondensable gases, but investigates the effects of vapor compressibility in a high temperature thermosyphon that can be significant in some cases.

## 3 Proposed Model

A model for high temperature thermosyphons operating in steady state conditions is proposed with the objective of predicting the thermal performance of this device. For modeling purposes, the thermosyphon is divided into seven regions, as shown in Fig. 1. Region 1 encompasses the condensed liquid film in the

inner surface of the condenser wall. Region 3 includes the liquid film that is in contact with the evaporator internal wall. Region 2, located within the adiabatic region, is considered thermally insulated from the environment. It includes the condensed liquid, which leaves the condenser. Region 4 encompasses the liquid pool under the effect of the incoming heat. The vapor inside the thermosyphon is considered to be within Region 5. All the noncondensable gases eventually present in the system are considered to be within Region 6. Finally, Region 7 includes the metallic pipe wall.

**3.1 Liquid Film.** Not many studies for heat transfer related to flow of condensed metal inside vertical tube walls can be found in the literature. In the present paper, a model based on the classical Nusselt theory is considered. It is assumed that the ratio between the film thickness and tube diameter is very small ( $\delta/d \ll 1$ ). Consequently, the inside vertical tube wall is considered a flat vertical surface. The condensed film is returned to the condenser by means of gravity. The vapor is assumed to be at the saturated temperature, and no shear forces are considered.

The Nusselt theory assumes laminar flow, constant properties in the film liquid, pure vapor with uniform temperature ( $T_{\text{sat}}$ ), and no shear stresses in the liquid-vapor interface. The mean heat transfer coefficient of the film,  $\bar{h}_L$ , is determined by the integration of local heat transfer coefficient,  $h_x = k/\delta$ , over the condenser length,  $L_c$ , resulting in:

$$\bar{h}_L = \frac{1}{L_c} \int_0^{L_c} h dx \rightarrow \bar{h}_L = 0.943 \left[ \frac{\rho_l g (\rho_l - \rho_v) h'_{lv} k_l^3}{\mu_l (T_{\text{sat}} - T_w) L_c} \right]^{1/4} \quad (1)$$

where  $h'_{lv} = h_{lv} + 0.68 C_{pl} (T_{\text{sat}} - T_w)$ , and  $C_{pl}$  is the liquid heat capacity. The properties of the liquid are evaluated at the average temperature between the wall and the vapor.

In the adiabatic section, the equations derived from the Nusselt analysis are not applied to the adiabatic section because there is no radial heat transfer in this region. The axial heat conduction is relatively small due to the small wall tube thickness and to the low thermal conductivity of its material. Then, the thickness of the liquid film is uniform and is the same as that which leaves the condenser region.

In the evaporator section, the vapor temperature level is considered lower than the wall temperature. The film thickness in the evaporator ( $\delta_{La+Lc+\Delta x}$ ) and the film mean heat transfer coefficient ( $\bar{h}_{ef}$ ) are modeled based on the same Nusselt theory of condensation for a flat vertical surface and are given by the following equations, respectively:

$$\delta_{La+Lc+\Delta x} = \left[ \delta_{La+Lc}^4 + \frac{4k_l \mu_l (T_{\text{sat}} - T_w) (x - L_a - L_c)}{g \rho_l (\rho_l - \rho_v) h_{lv}} \right]^{1/4} \quad (2)$$

where  $\delta_{La+Lc}$  is the film thickness at the end of the adiabatic section.

**3.2 Liquid Pool.** In the liquid pool region, nucleate boiling is considered. For mercury, some correlations for the heat transfer coefficients of the pool were obtained from the literature, such as those of Subbotin [13] and Ratiani [14], given, respectively, by

$$h_{ep} = C_s (q^{2/3}) \left( \frac{k_l h_{lv} P_l}{\sigma T^2} \right)^{1/3} \left( \frac{P_l}{P_c} \right)^s \quad (3)$$

$$h_{ep} = \frac{0.007 k_l}{r_n} \left( \frac{q r_n^2 h_{lv} \rho_g}{\sigma T_{\text{sat}} k_l} \right)^{7/10} \left( \frac{\rho_l \sigma T_{\text{sat}} C_{pl}}{h_{lv}^2 \rho_g^2 r_n} \right)^{1/4} \times \left( \frac{r_n P^{1/2} (\rho_g^{-1} - \rho_l^{-1})^{1/2}}{\mu_l / \rho_l} \right)^{1/4} \quad (4)$$

where  $C_s = 8.0$  and  $s = 0.45$  for  $P_l/P_c < 0.001$ ,  $C_s = 1.0$  and  $s = 0.15$  for  $P_l/P_c \geq 0.001$ ,  $P_c$  is the critical pressure of fluid,  $P_l$  is the liquid pressure in contact with heated surface,  $r_n$  is the radius

of the nucleation site (equals  $20 \times 10^{-6} \text{ m}^2$ , characteristic of industrial surfaces), and  $T$  is the average between saturation ( $T_{\text{sat}}$ ) and wall ( $T_w$ ) temperatures, in Kelvin.

**3.3 Vapor Region.** This region encompasses the nucleus of evaporator, condenser, and adiabatic sections, where the vapor is located. The vapor is assumed to be at the saturated temperature level and at the same temperature along the pipe. Vieira da Cunha [15] presented a model for the vapor pressure distribution inside the tube, which can be applied to the vapor region of thermosyphon. He concluded that the vapor pressure difference between condenser and evaporator is negligible for the mercury thermosyphon under investigation. Then, in the present model, no vapor pressure or temperature distributions are considered. Vapor entrainment in any of the thermosyphon regions, due to liquid drag forces, is not considered. This means that no shear stresses are considered, in accordance with Nusselt's model hypothesis. All vapor produced in the evaporator is considered condensed in the condenser.

**3.4 Noncondensable Gas Region.** The present model also considers the noncondensable gases, which can be eventually found inside the thermosyphon. The major problem is to determine the amount of noncondensable gases. During the fabrication process, the tube is cleaned and evacuated before the addition of the working fluid. The noncondensable gases are generally formed from the chemical reaction between the fluid and the tube material. The volume of these gases is hard to predict. In the present model, only the noncondensable gases (air, for instance), remaining after vacuum is created inside the tube, is considered. In other words, the fluid is considered completely compatible with the tube material not producing noncondensable gases.

Noncondensable gases are clustered in the upper condensation region during operation, decreasing the effective length of the thermosyphon. Actually, in the regions where the noncondensable gases are present, the heat transfer coefficient inside the tube decreases significantly because condensation no longer happens inside the tube. Furthermore, it is well known that the capacity of exchanging heat in gases is very limited. As a result, in present model the noncondensable gas region is considered adiabatic.

For modeling this region, the pressure, the mass, and the temperature of these gases in the start-up conditions are considered known. In steady state conditions, the final volume of the noncondensable gases are obtained from the ideal gas law, considering that the temperature of the gas is known, as well as the pressure, which is considered the same as the vapor pressure in the upper part of the condenser region. Actually, the model is a design tool, and this region was included to help in the adjustment of the theoretical model to experimental data that will be eventually available.

**3.5 Distribution of Wall Temperature.** The temperature distribution of the thermosyphon wall is determined through the method of finite volumes [16]. In this method, the wall is divided into several small volumes, where a balance of energy, for steady state conditions, is performed. Each volume consists of a ring of thickness  $\Delta x$ , as illustrated in Fig. 2. The differential volume of temperature  $T_p$  is submitted to the following heat flux ( $q$ ) through the boundary areas: conduction from north ( $n$ ) and south ( $s$ ) and convection for east ( $e'$ ) and west ( $w'$ ) side areas. The volume is in contact with outside and inside fluids at temperature levels of  $T_o$  and  $T_i$ , respectively, where  $T_o$  is the environmental temperature, considered uniform for each section, while  $T_i$  is assumed at the vapor or pool temperatures, depending on the region of the thermosyphon. The following finite volume equation resulted from this balance for each volume:

$$A_p T_p = A_n T_N + A_s T_S + B \quad (5)$$

where the coefficients are given by:  $A_p = h_w A_{w'} + A_s + A_n + h_e A_{e'}$ ,

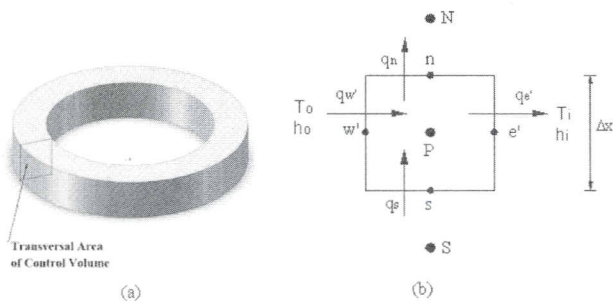


Fig. 2 (a) Control volume and (b) energy balance in the cross-sectional area of the control volume

$$A_s = (k_w A_{xs}) / \Delta x, A_n = (k A_{xn}) / \Delta x, \text{ and } B = h_w A_w T_o + h_e A_e T_i.$$

Equation (5) is applied to each control volume of the thermosyphon wall. All the equations together form a system of linear equations, which is solved by means of iterative methods. An initial temperature guess is applied to all the volumes, and the temperature, for the  $k+1$  iteration, is related to the temperature of the  $k$  iteration by the following self-adjustable equation, according to the Gauss-Seidel [16] method:

$$A_p T_p^{k+1} = A_s T_s^{k+1} + A_n T_N^k + B \quad (6)$$

The heat transfer coefficient inside the tube depends on the thermosyphon region under consideration. As already mentioned, two subregions are found in the evaporator region: the pool and the falling liquid film. Equation (2) is used for the falling liquid subregion, and Eq. (3) or Eq. (4) for the pool subregion, depending on whether the volume is in contact with the falling film or with the pool. In the condenser, the internal heat transfer coefficient is given by Eq. (1) for each control volume.

The outside face of the wall receives a uniform heat flux rate ( $Q_w$ ) in the evaporator. Then, the coefficients  $A_p$  and  $B$  of Eq. (5) for this region turns out to be  $A_p = A_s + A_n + h_e A_e$ , and  $B = Q_w + h_e A_e T_i$ . For the condenser, the outer heat transfer coefficient is calculated by experimental data or through appropriate correlations of literature.

**3.6 Numerical Solution.** As already mentioned, the model is solved numerically by means of an iterative process using FORTRAN. The input data for the model are: lengths of the condenser ( $L_c$ ), adiabatic section ( $L_a$ ), and evaporator ( $L_e$ ); mass of fluid; external heat transfer coefficients; condenser external wall temperature; tube inner diameter ( $d_i$ ); and heat transfer rate ( $\dot{Q}$ ). The model determines the wall temperature distribution and the film thickness of the thermosyphon for steady state conditions. A check of the minimum amount of fluid to guarantee that the entire internal wall is in contact with the condensate film is performed by comparing the calculated mass of condensate film with total working fluid mass of thermosyphon.

First, the model calculates the effective length of thermosyphon, defined as the region where there is significant exchange of heat (in other words, the region not in contact with the noncondensable gases). Then, the effective length of thermosyphon is divided into several control volumes. The energy equilibrium equations for each control volume, including the heat transfer coefficients and liquid film thickness, were obtained according to the seven regions (see Fig. 1), using the formulation presented in the last section. These control volume equations are solved numerically based on the method of finite volumes [16].

The whole tube is initially considered at uniform temperature in the design working temperature level. This temperature basically depends on the amount of heat that the device is supposed to transfer. A good initial guess reduces the computational time so that the convergence is obtained after a few hours of computation. The convergence is considered achieved when the comparison

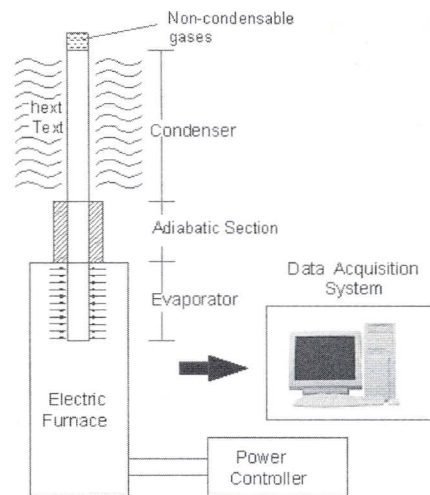


Fig. 3 Schematic of the experimental apparatus

between the heat transfer rate numerically calculated and the input data is within an established tolerance. When these values are unbalanced, the vapor temperature, which is considered uniform along the whole tube, is adjusted; decreased, if the heat output is larger than the heat input or increased if the heat output is lower than the heat input.

## 4 Experimental Work

**4.1 Experimental Setup.** The experimental apparatus is composed by an electric furnace, a power controller, and a data acquisition system, as illustrated in the schematic in Fig. 3. The furnace contains three blocks of electric resistances, each one 200 mm in length and 50 mm in diameter. Each resistance has a digital temperature controller that keeps its temperature above the maximum value of 1200°C. The resistances transfer heat to the evaporator section through radiation. This furnace is isolated by ceramic fiber. In addition, a box of wood with vermiculite (natural mineral) is built around it to minimize the heat loss through the walls. A device located at the top of the furnace, consisting of four adjustable connecting rods, is built to support the pipe, so that the thermosyphon remains upright.

The heat flux rate, which is dissipated by the resistances, is regulated by a power controller that varies the voltage to up to 220 V. The voltages and temperatures are measured by a data acquisition system (HP 34970 Bench-Link Data Logger), and the resulting data are stored in a computer.

The test laboratory is open to the environment, as a safety procedure concerning the use of mercury. Therefore, the condenser region room temperatures and external heat transfer coefficients are not controlled, and depend on the environmental conditions. The external heat transfer condenser coefficients employed in this work are obtained from experimental data.

**4.2 Description of Thermosyphons.** Two devices, Thermosyphon A and Thermosyphon B, were designed, constructed, and tested. Both are made of stainless steel 316L tubes, with a length of 1.0 m, and outer and inner diameters of 25.4 mm and 21 mm, respectively. The condenser region of Thermosyphon A of approximately 500 mm has 31 fins with a diameter of 50 mm, which are 14.6 mm distant from each other. Thermosyphon B is smooth in all regions. The amount of mercury used was approximately 30.5 ml for Thermosyphon A and 40 ml for Thermosyphon B.

Inside both thermosyphons, a small diameter tube (capillary tube) is located in the central axis and welded to the cap of the thermosyphons. The region between these inner and outer tubes is sealed. A thermocouple, which slides through the capillary tube,

**Table 2 Specification of tests for the thermosyphons**

Description	Thermosyphon A (finned condenser)		Thermosyphon B (all smooth)	
	Heat transfer rate	Condenser length	Evaporator length	Adiabatic section length
Heat transfer rate	485 W	1609 W	486 W	1922 W
Condenser length	700 mm	690 mm	640 mm	640 mm
Evaporator length	200 mm	210 mm	200 mm	200 mm
Adiabatic section length	100 mm	100 mm	140 mm	140 mm
Filling ratio	48.5%	48.5%	63.5%	63.5%

measures the vapor temperature. The material of the small tube is stainless steel 316L, with an outer diameter of 6.35 mm and a thickness of 1.0 mm.

An analysis of heat losses by conduction through the capillary tube was performed, showing that they are negligible and that the temperature readings inside the tube are good measurements of the vapor or liquid pool temperatures (depending on the position of the thermocouple inside the capillary tube).

**4.3 Experimental Methodology.** The thermosyphons were instrumented with K-type thermocouples manufactured by OMEGA. These thermocouples were spot welded on the external wall of the tube to guarantee good contact with the wall and, consequently, good measurements of temperature. The thermocouples are protected against the radiation and convection through aluminum strips.

Another thermocouple was inserted inside the capillary tube to monitor the vapor temperature along the entire length of thermosyphon. This K-type thermocouple 1.5 m in nominal length is manufactured by ECIL. The thermocouple has an external protection consisting of a sheath of stainless steel, with mineral as insulation between the wire and the aluminum. The tests were conducted in steady state conditions that were considered reached after several operation hours, when the temperature variation was less than 9°C in all thermocouples. Then, the data acquisition system was used to acquire data in regular time intervals of 10 s. The descriptions of the thermosyphons tested (condenser, evaporator, and adiabatic section lengths), as well the power inputs applied in each test, are found in Table 2.

**4.4 Experimental Results.** The data collected from the tests allow for the plot of Thermosyphons A and B external and internal temperature profiles. The heat transfer rate for each thermosyphon ( $\dot{Q}$ ) is determined by the difference between power dissipated by the electric furnace resistances and the heat losses from the furnace to the environment. In the present case, the heat losses through the furnace walls are considered negligible, which is a good hypothesis, considering the vermiculite insulation around the furnace. Then, the heat transfer rate is calculated by the well known equation, where  $V$  is the electrical potential applied to the electric resistance  $R$ .

An analysis of the uncertainty of the temperature measurements and of the heat transfer rate was carried out. An accuracy of  $\pm 2$  W was obtained for the 485 W and 486 W power inputs and of about  $\pm 8$  W for the 1609 W and 1922 W power inputs. Accuracies of around  $\pm 8.2^\circ\text{C}$  are estimated for temperatures from  $200^\circ\text{C}$  to  $600^\circ\text{C}$  and of  $\pm 8.9^\circ\text{C}$  for temperatures from  $600^\circ\text{C}$  to  $1000^\circ\text{C}$ . This relatively high uncertainty was also observed by White [17], who reports nonuniform temperature measurements related to high temperature levels and installation problems.

Figure 4 shows the wall and vapor temperature profiles for Thermosyphon A (finned in the condenser region), with heat transfer rates of 485 W and 1609 W, respectively. Temperature measurement uncertainties are also presented in these figures for each point, through vertical bars. In Fig. 4, it can be noted that in almost the whole tube, the vapor temperature levels are higher than the wall temperature, but an intersection of these curves is observed for the 0.8 m position (condenser). Actually, the sudden

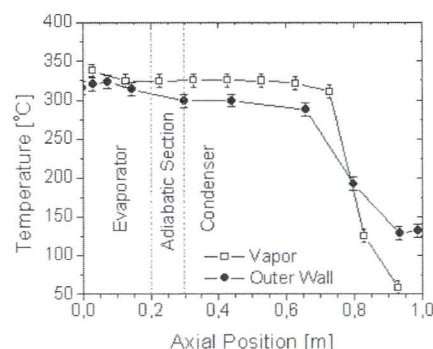


**Fig. 4 Temperature profile of Thermosyphon A subjected to 485 W of heat power**

temperature drop shows the region where the noncondensable gases concentrate at the tip of the condenser. In this region, the heat exchange between gases and tube is very poor, and the heat conduction through the solid materials takes the major role. One should note that the axial heat conduction through the thermosyphon wall is much higher than the axial conduction of the inner capillary tube wall, whose thickness is much thinner than the thermosyphon wall.

The outer wall temperatures should be lower than vapor temperatures (capillary tube) in the condenser region because the heat leaves the thermosyphon in the radial direction. On the other hand, in the evaporator, which is a region where the tube receives heat, the outer wall temperatures should be higher than the vapor temperatures. The plots show this trend but also show that there are some points in the evaporator where the inverse is observed (see Fig. 4). This is an unexpected behavior, which is attributed to the problem related to high temperature measurements, as already observed. Despite this inconsistency, it is important to emphasize that these differences between vapor internal (capillary tube) and external (outer wall) temperatures, also considering the difference of temperature in thickness wall, are within the uncertainty of temperature measurements. Due to its problem, many measurement repetitions and parallel experimental studies, not shown in this paper, were conducted (Fig. 5).

For Thermosyphon B, which has no fins, two tests were also performed, as show in Table 2. Figure 6 shows the tube wall and vapor temperature profiles for these tests, for heat transfer rates of 486 W and 1922 W, respectively. The experimental points of these plots also present vertical bars, representing the experimental uncertainties. It can be noted, in both cases (Fig. 6), that the outer wall temperatures are higher than the vapor temperatures along the tube. It was expected that, in the condenser region, the vapor temperature should be higher than the wall temperatures, but this is not verified by the data. On the other hand, one should note that,

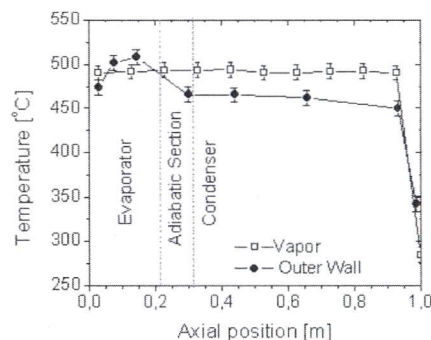


**Fig. 5 Temperature profile of Thermosyphon A subjected to 1609 W of heat power**

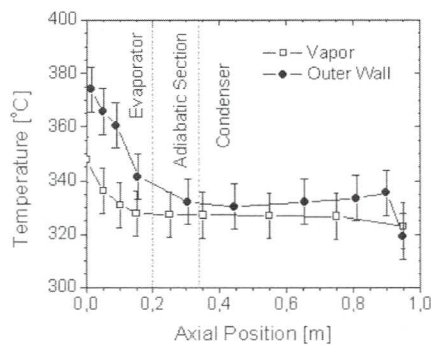


Fig. 6 Temperature profile of Thermosyphon B subjected to 486 W

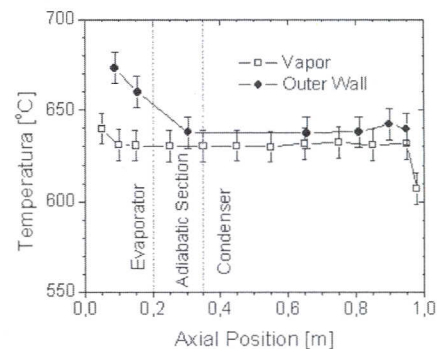


Fig. 7 Temperature profile of Thermosyphon B subjected to 1922 W

again, the temperature differences between wall and vapor in this region are within the temperature measurement uncertainties, also considering the conduction radial temperature difference.

The wall temperature for Thermosyphon A, which is finned, is compared with the wall temperature profile of Thermosyphon B, which is smooth, for a similar level of heat transfer rates. It is observed that the outer wall temperature profile for Thermosyphon A (finned) is lower than for Thermosyphon B (smooth), as expected, since the finned region promotes a better heat exchange with the environment, decreasing the temperature levels. In addition, the temperature differences between the two thermosyphons increase when the power increases due to the same reasons. It can also be observed that the region occupied by noncondensable gases is larger for Thermosyphon B because the lower levels of temperature lead to lower vapor pressures, causing a minor compression of these gases.

The radial differences of temperature can be significant, due to the low thermal conductivity of the wall tube. This radial thermal resistance represents the largest individual resistance of the overall thermal resistance circuit of thermosyphon ( $R_t$ ). The thermal resistance, which represents the capacity of the device to transfer heat, is given by

$$R_t = \Delta \bar{T} / \dot{Q} \quad (7)$$

where  $\Delta \bar{T}$  is the mean temperature difference between the condenser and evaporator. It can be noted that the thermal resistance decreases with the heat transfer rate increase. The thermal resistance of Thermosyphon A, for 485 W, is smaller than that for Thermosyphon B, for 486 W (note that the power is practically the same). Two facts may have contributed to a lower thermal resistance of Thermosyphon A: the smaller filling ratio of Thermosyphon A and the presence of fins, which provides better heat exchange in the condenser external area.

## 5 Comparison Between Theoretical and Experimental Results

The model presented in Sec. 4 was implemented in the computer using thermophysical and geometric properties of Thermosyphons A and B, shown in Table 2, and compared with the experimental temperature distribution of the outer wall.

Only the gases that remain after the tube evacuation were considered as the noncondensable gases in the present simulation. A remaining pressure of 100 Pa was assumed after the evacuation. The perfect gas model showed that the tube length occupied by the noncondensable gases is negligible. However, in actual cases, other noncondensable gases are formed, mainly due to the chemical reaction between the fluid and tube. As already discussed, they can occupy a considerable volume, especially when the temperature level is low for low heat power transport, as observed in Fig.

4, for Thermosyphon A. Therefore, all model simulations were performed considering only the effective length of the thermosyphons tested (Fig. 7).

The results for Thermosyphon A for 485 W are compared with the proposed model, for the two pool correlations, in Fig. 8. A good comparison of the temperature profiles resulting from the simulation and experimental data is observed in the condenser and the liquid film region of evaporator. In the liquid pool, levels of temperatures are different for the two simulations. Observing Fig. 8, one can note that the model with Ratiani correlations shows a step in the temperature profile of the evaporator region, while the model with the Subbotin correlation shows a much smoother behavior. Obviously, this happens because the values of the pool heat transfer coefficients obtained from Ratiani are lower than those of Subbotin's correlation. The temperature data in this region present a higher level than the model, therefore, the model with the Ratiani correlation has better comparison with data.

In Fig. 8, it can be observed that, in the adiabatic section, there is a linear variation in temperature for both models because in this region only the axial heat conduction by the wall of thermosyphon is considered. The models used to determine the temperature distribution of the evaporator liquid film, adiabatic, and condenser regions are the same for both theoretical plots.

The outer wall temperature profiles for dissipations of 486 W and 1922 W, for Thermosyphon B, were also simulated using both theoretical correlations for the pool heat transfer coefficients. Figure 9 presents the comparison between models and data for these profiles. The observations made for the thermal behavior of Thermosyphon A are valid here; again the theoretical model employing the Ratiani correlation presents reasonable comparison with data for the evaporator region, while the comparison between the model and data is very good for the rest of the thermosyphon.

In general, the theoretical temperature profiles show a uniform (constant value) distribution in the condenser, in the pool region, and in the evaporator liquid film region, and a linear profile in the adiabatic section. The linear profile of adiabatic section is justified only by the presence of the axial conduction of the wall. The

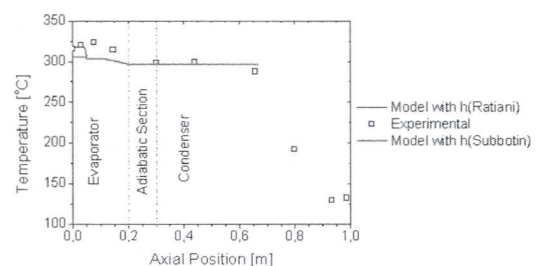
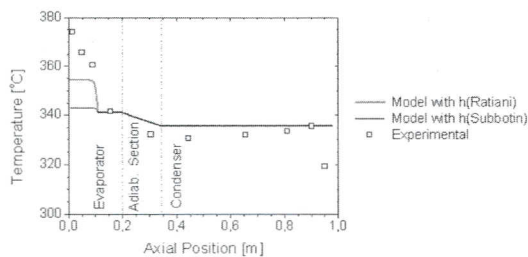


Fig. 8 Comparison: experimental data and model for Thermosyphon A to 485 W



**Fig. 9 Comparison: experimental data and model for Thermosyphon B to 486 W**

uniform profile in other regions shows uniform heat transfer coefficients, both in the pool and in the liquid film regions. Actually, these profiles are combinations of the internal and external heat transfer coefficients, connected to the low axial thermal resistance of the tube wall. These facts show that the accuracy of model is essentially related to the precision with which heat transfer coefficients are determined.

## 6 Conclusion

This paper presents a theoretical and experimental study of mercury thermosyphons. The outer wall and vapor temperature profiles, as well as the thermal resistance, were shown for two distinct thermosyphons: Thermosyphon A, which is finned in the condenser, and Thermosyphon B, which is all smooth. The outer temperatures, measured on the external surface of tube, are lower for the Thermosyphon A, and the difference in these temperatures between the two thermosyphons increases when the level of power also increases.

In both thermosyphons, the difference in mean temperature between the condenser and evaporator is significant due to the high thermal resistances of the wall in the radial direction, as the material of this wall (stainless steel 316L) presents low thermal conductivity and relatively thick walls.

Data obtained from experimental tests of mercury thermosyphons were confronted with theoretical results from the proposed model, through the comparison of the outer wall temperature profiles. The simulations were conducted using two different correlations for the pool heat transfer coefficients: Subbotin [13] and Ratiani [14] correlations. The uniform temperature profiles for the condenser and evaporator liquid film regions are due to the uniform characteristics of the heat transfer coefficients. The two steps found in the evaporator theoretical temperature distribution curves are because the pool and the liquid film regions present two uniform and different levels of heat transfer coefficients.

Within the regions, the uniformity is possible because the heat transfer coefficients inside the thermosyphon are much higher

than that due to the tube wall material. A good choice of the heat transfer coefficient correlations is very important for a good theoretical model.

For the present studied cases, the comparison between the experimental data and theoretical temperature profiles is good, especially in the condenser and adiabatic sections. In the evaporator, this comparison is poorer, independent of the theoretical correlation used for the determination of the heat transfer coefficient. Even when considering this poorer comparison, the model was shown to be very reasonable and can be used as major tool for the design of liquid metal thermosyphons for industrial applications.

## References

- [1] Vieira da Cunha, A. F., and Mantelli, M. B. H., 2006, "Modeling of High Temperature Thermosyphons," Ninth AIAA/ASME Joint Thermophysics and Heat Transfer Conference, San Francisco, CA.
- [2] Ranken, W. A., and Lundberg, L. B., 1978, "High Temperature Heat Pipes for Terrestrial Applications," Third International Heat Pipe Conference, CA, May 22–24.
- [3] Merrigan, M. A., 1981, "Heat Pipes for High Temperature Industrial Waste Heat Recovery," Eighth Energy Technology Conference, Washington, DC.
- [4] Yamamoto, T., Tanaka, Y., Sasaki, M., and Hatori, H., 1982, "Study on Life of Sodium Heat Pipe," *J. Heat Recovery Syst.*, **2**(4), pp. 369–376.
- [5] Yamamoto, T., Nagata, K., Katsuta, M., and Ikeda, Y., 1994, "Experimental Study of Mercury Heat Pipe," *Exp. Therm. Fluid Sci.*, **9**, pp. 39–46.
- [6] Reid, R. S., Sena, J. T., and Merrigan, M. A., 1999, "Transient Tests of a Molybdenum-Lithium Heat Pipe," 11th International Heat Pipe Conference, Tokyo, Japan.
- [7] Park, S. Y., and Boo, J. H., 2004, "An Experimental Study on the Heat Transfer Characteristics of High-Temperature Cylindrical Heat Pipes," *Korean Journal of Air-Conditioning and Refrigeration Engineering*, **16**(1), pp. 70–76.
- [8] Reed, J. G., 1985, "Analytical Modeling of the Two-Phase Thermosyphon," Ph.D. thesis, Department of Mechanical Engineering, University of California, Berkeley, CA.
- [9] Reed, J. G., and Tien, C. L., 1987, "Modeling of the Two-Phase Closed Thermosyphon," *ASME J. Heat Transfer*, **109**(3), pp. 722–730.
- [10] Storey, J. K., 2003, "Modeling the Transient Response of a Thermosyphon," Ph.D. thesis, Department of Mechanical Engineering, Brigham Young University, Provo, UT.
- [11] Ling, J., and Cao, Y., 2000, "Closed-Form Analytical Solutions for Radially Rotating Miniature High-Temperature Heat Pipes Including Non-Condensable Gas Effects," *Int. J. Heat Mass Transfer*, **43**(19), pp. 3661–3671.
- [12] Harley, C., and Faghri, A., 1994, "Complete Transient Two-Dimensional Analysis of Two-Phase Closed Thermosyphons Including the Falling Condensable Film," *ASME J. Heat Transfer*, **116**, pp. 418–426.
- [13] Carey, V. P., 1992, *Liquid-Vapor Phase-Change Phenomena: An Introduction to the Thermophysics of Vaporization and Condensation Processes in Heat Transfer Equipment*, Taylor & Francis, London.
- [14] Bullerschen, K.-G., and Wilhelm, H., 1991, "Cooling of Arc Furnace Electrodes With Heat Pipes," *Chem. Eng. Technol.*, **14**, pp. 45–53.
- [15] Vieira da Cunha, A. F., 2008, "Análise de Termossifões que operam em Altas Temperaturas," MS thesis, Mechanical Engineering Department, Federal University of Santa Catarina.
- [16] Maliska, C. R., 1995, *Transferência de Calor e Mecânica dos Fluidos Computacional*, LTC.
- [17] White, D. R., 2005, "Calibration and Standards in Temperature Measurement," *Handbook of Measuring System Design*, P. H. Sydenham and R. Thorn, eds., Wiley, New York.